

FcRn-targeting and ROS-responsive Fedratinib-incorporated Nanoparticles Alleviate Asthma by Inducing Eosinophil Apoptosis

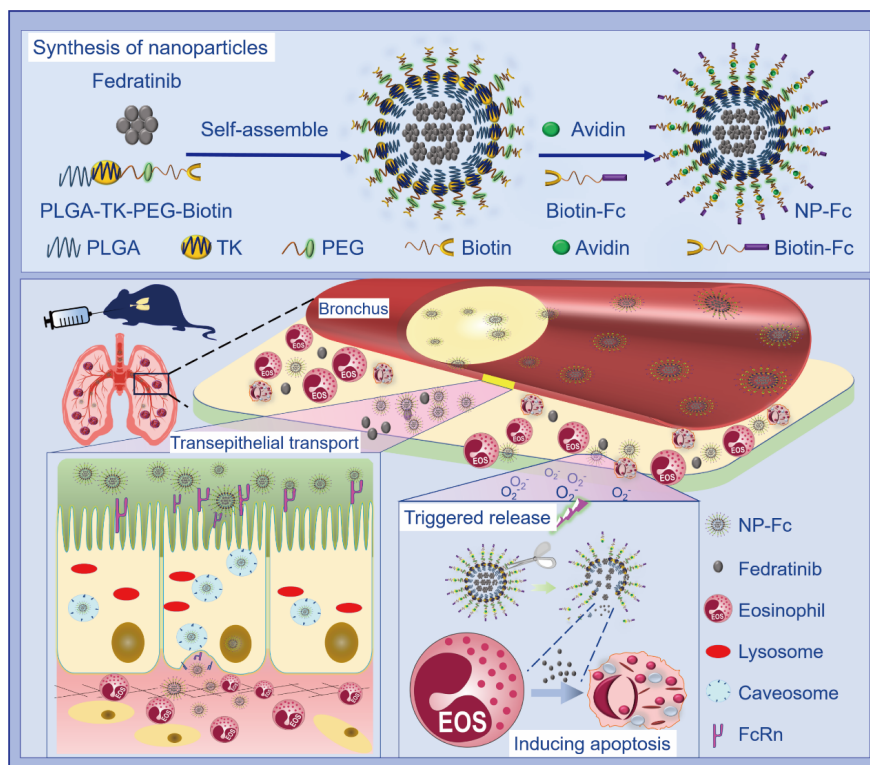
Weimin Sun¹, Shijie SONG¹, Guangmeng LI¹, linghui ZHOU¹, Junmou XIE¹, Yuhe GUO¹, Jun ZENG¹, Junyan Zhang¹, Linmei LI¹, Jie Yan¹, Xintao SHUAI¹, and Ailin TAO¹

¹State Key Laboratory of Respiratory Disease

May 14, 2022

Abstract

Background: Reducing the number of airway eosinophils is critical for treating eosinophilic asthma. The JAK2-STATs pathway is essential for myelopoiesis of eosinophils and production of type I and II cytokines, and therefore can be a novel target for intervention of eosinophilic asthma. Here, we aimed to demonstrate the apoptosis-inducing potential of Fedratinib (FDTN), a JAK2-specific inhibitor, and test the efficacy of the ROS-responsive, FcRn-targeting and FDTN-caged nanoparticles on eosinophilic asthma alleviation. **Methods:** The apoptosis-inducing potential of FDTN in eosinophils from asthma patients was assessed by flow cytometry, and light and electron microscopy. FDTN-caged nanoparticles (NPs-FDTN) were designed to ROS responsive and modified with Fc portion of IgG through the avidin-biotin interaction. The biological availability of NPs-FDTN was assembled via biochemical and immunological analysis, and the therapeutic effects were investigated in eosinophilic asthma model mice by comparing free FDTN and budesonide treatment. **Results:** FDTN blocked the JAK2/STAT5 pathway and activated the intrinsic pathway of apoptosis in eosinophils in a concentration-dependent manner. NPs-FDTN crossed the epithelial barrier via the Fc/FcRn-mediated transcytosis, bypassed the lysosome and entered the inflammatory microenvironment. Caged FDTN was released from the nanoparticles in the presence of ROS. Compared to free FDTN, the residence time of FDTN in the lung parenchyma was prolonged and the therapeutic effects were improved when delivered in nanoparticles. **Conclusion:** Ros-responsive, FcRn-targeting and FDTN-caged nanoparticles overcame the airway epithelial barrier and improved the bioavailability on eosinophil apoptosis. This study provides a fancy and safe therapeutic strategy for treatment of eosinophilic asthma.



1. Introduction

Asthma is a common chronic inflammatory airway disorder that causes a significant socioeconomic burden.¹ Among the asthma endotypes, eosinophilic asthma with the type 2 immune response is most common.^{2,3} Previous studies demonstrated that eosinophils play a causal role in the pathogenesis⁴⁻⁷ by releasing multiple pro-inflammatory mediators.^{8,9} The cytokine-activated Janus kinase-signal transducer and activator of transcription (JAK/STAT) signaling cascade plays an important role in the control of immune responses.^{10,11} Asthma-relevant cytokines (IL-3, IL-5, IL-4, IL-13, granulocyte-macrophage colony stimulating factor (GM-CSF) and thymic stromal lymphopoietin (TSLP)) exacerbate asthma pathology by promoting eosinophil recruitment and survival, airway hyperresponsiveness, mucus production, and immunoglobulin class switching through the JAK/STAT pathway.^{12,13} Therefore, two major strategies have been developed to inhibit the JAK/STAT pathway: antibodies against type 2 cytokines and small molecule inhibitors of JAK. Among asthma treatment regimen, anti-IL-4/-5/-13, and anti-TSLP antibodies have complemented glucocorticoids (GCs).¹² However, some severe asthma patients display steroid resistance and long-term use of inhaled GCs causes adverse effects.¹⁴ IL-5-blocking antibody, such as Mepolizumab, can reduce airway eosinophil numbers, but not attenuate completely their functional phenotype, which causes limited efficacy in asthmatic patients.¹⁵ Thus, there is an unmet medical need for effectively repressing or controlling lung inflammation.

IL-5, IL-3 and GM-CSF bind to the receptors on the eosinophils to activate the JAK/STAT pathway, and share the common downstream of tyrosine kinase, JAK2.^{16,17} Fedratinib (FDTN) is a highly selective JAK2 inhibitor¹⁸ authorized by Food and Drug Administration (FDA) for treatment of bone marrow fibrosis.¹⁹ Therefore, considering its mode of action, we envisioned that FDTN has great potential to be used to alleviate asthma.

Generally, asthma treatment agents are delivered via oral administration, aerosol inhalation, or intravenous injection. Different delivery routes face different challenges such as harsh acidic pH in the stomach and enzymatic digestion in the intestines, bioavailability, pharmacokinetics, and epithelial or blood-brain barriers²⁰.

FDTN is a poor solubility and hydrophobic small molecule.¹⁹ The clinical application of FDTN faces the same limitations, such as poor solubility, short half-life in circulation, and off-target effect.

Over the past decades, polymeric nanocomplexes have been used as a molecular Trojan horse to deliver drugs to the sites of diseases such as asthma²¹ and to realize the release them by using the microenvironmental conditions such as pH,²² exposure to enzymes,²³ and reactive oxygen species (ROS),²⁴ or artificial means such as near infrared (NIR) light.²⁵ Neonatal Fc receptor (FcRn)-mediated transcytosis has been plotted as a strategy to increase the shuttle of drugs across the epithelial cell layer.²⁶ Adult human and mouse lung bronchial epithelial cells also express FcRn.²⁷ During asthma, there is a high level of reactive oxygen species (ROS) in the airway microenvironment and eosinophils are the main source of ROS.^{28,29}

In the present study, we encapsulated FDTN into Fc-modified and ROS-responsive nanoparticles (NPs-FDTN) to deliver it across the airway transepithelial barrier and then release it at the sites of abnormally elevated ROS in the inflammatory lung. Firstly, FDTN was proved to promote apoptosis of eosinophils in vitro and attenuate allergic airway inflammation in vivo. In ovalbumin (OVA)-induced Th2 allergic airway inflammation mice models, it was evidenced that NPs-FDTN can suppress inflammation significantly better than free FDTN. Moreover, there was no liver and kidney damage, most likely due to FDTN retention in the lung.

2. Materials and methods

2.1 Human peripheral blood eosinophil isolation and stimulation

All samples of asthma patient were derived from leftover diagnostic samples from patients. The patients provided informed consent to the study, which was approved by Institutional Research Ethics Committee of the Second Affiliated Hospital of Guangzhou Medical University (Approval No. 2019-ks-18). The asthma patients were diagnosed according to Global Initiative for Asthma guidelines.

The peripheral blood eosinophils of asthma patients were isolated and purified according to previously described.⁷ In brief, 10 mL heparinized blood was diluted and mixed well with 10 mL PBS buffer (pH7.4). Granulocytes and erythrocytes were separated from mononuclear cells by density gradient centrifugation on Ficoll-Hypaque solution (LTS1077, Haoyang, Tianjin). Erythrocytes were lysed by lysing solution (BD FACS) and discarded. Eosinophils were purified from granulocytes by a commercial CD16 immunomagnetic negative selection eosinophil isolation kit. (#17956, STEMCELL). The eosinophil purity (>98%, **Figure 1F**) was confirmed by the Wright-Giemsa stain method. The purified eosinophils were seeded in 100 μ L medium (RPMI 1640 with 10% FBS) in 96-well cell plates (2×10^4 cell per well) and treated with gradient concentrations of FDTN (2.5, 5.0, 10.0 μ M) (TG-101348, MCE) at 37 °C in 5% CO₂ for 18 h or vehicle control as described in the figures.

2.2 Determination of cell viability, apoptosis, and caspase 3 activation

The purified eosinophils were co-cultured with FDTN, light microscopy and transmission electron microscope (TEM) (JEOL JEM1400plus, Japan) were applied to assess the apoptotic eosinophil morphology, the flow cytometry (fluorescein isothiocyanate-Annexin V(AnnV) and PI) was used to detect the early apoptosis (AnnV⁺/PI⁻) and post-apoptotic necrosis or late apoptosis (AnnV⁺/PI⁺). Cell viability was analyzed by a Cell Counting Kit-8 (CCK-8, Beyotime, Shanghai, China), and lactate dehydrogenase (LDH) in the cell-free supernatant was assayed by the automatic biochemical analyzer (cobas®8000 Automatic biochemical analyzer, ROCHE) according to the manufacturer's protocol. The FDTN treated eosinophils were permeabilized with Perm/Fix solution (554714, BD) and stained with Anti-cleaved caspase-3 (ab2302, Abcam,) according to the manufacturer's protocols, finally analyzed with flow cytometry. Eosinophils were lysed and performed for Western blotting of cleaved caspase-3.

2.3 Assessment of p-STATs in eosinophils

The gradient concentrations of FDTN (2.5, 5.0, 10.0 μ M) treated eosinophils were permeabilized with Perm/Fix solution and stained with antibodies against p-STAT3(#Py705, BD), p-STAT5 (#Py694, BD) and

p-STAT6 (#Py641, BD) according to the manufacturer's protocols, finally analyzed with flow cytometry.

2.4 Western blot of JAK2, p-JAK2, STAT5 and p-STAT5

The gradient concentrations of FDTN (2.5, 5.0, 10.0 μM) treated eosinophils were washed once in cold PBS and lysed in RIPA buffer with protease and phosphatase inhibitor cocktails (Roche, Mannheim, Germany). Protein concentrations were determined by the BCA assay. The extracts were mixed with 5 x SDS loading buffer at 100 °C for five min. The samples were separated by 10% SDS-PAGE and transferred onto nitrocellulose membranes. The membranes were blocked with 5% nonfat milk for 1 hour. After washing, membranes were incubated with primary antibodies (anti-JAK2, anti-p-JAK2, anti-STAT5 and anti-p-STAT5) overnight at 4 °C, and then incubated with the appropriate secondary antibodies. The active bands were exposed to chemiluminescence. GAPDH was used as a protein loading control. The anti-JAK2 (D2E12), anti-p-JAK2 (Tyr1007/1008) anti-STAT5 (D2O6Y) and anti-p-STAT5 (Tyr694) were purchased from Cell Signaling Technology (CST, Danvers, Mass).

2.5 BAD mitochondrial translocation

The FDTN (10.0 μM) treated eosinophils were gently suspended with 100 nM Mito-Tracker® Green FM staining solution preheated at 37 °C, then cultured at 37 °C in 5% CO₂ for 30 min. The cells were collected by centrifugation and re-suspended in PBS. Finally, the eosinophils were evenly thrown onto the slides by cell throwing technique. The slide cells were fixed with 4% paraformaldehyde for 10 min and then permeabilized with 0.5% Triton-X 100 and 3% BSA in PBS for 10 min. The cells were incubated with anti-BAD antibody (ab32445, Abcam) in PBS with 10% BSA at 4 °C overnight. The cells were then washed and incubated with Alexa Fluor 555-conjugated anti-mouse IgG (ab150114, Abcam). The stained cells were examined by using the fluorescence microscope.

2.6 Preparation of Nanoparticles

Biotin poly (L-lactide-co-glycolide)-thioketal-polyethylene glycol (Bio-PLGA-TK-PEG) were obtained from Xi'an ruixi Biological Technology (Xi'an, China). **Figure S4** showed the ¹H-NMR spectrum of the Biotin-PEG-TK-PLGA in CDCl₃. For making Bio-PLGA-TK-PEG encapsulated FDTN, modified single-emulsion (O/W) solvent evaporation method was used for the formation of the particles. Briefly, two mg of FDTN and 10 mg of Bio-PLGA-TK-PEG were dissolved in dichloromethane. The primary solution was added to 10 mL of 1% (*w/w*) PVA solution and further emulsified by sonication at 220 W for five min to obtain the emulsion (O/W). The final emulsion was evaporated under a vacuum to remove the organic solvent, and the colloidal solution was then centrifuged (12,000 rpm, 30 min) at 4 °C and washed three times with deionized (DI) water to remove PVA and the free FDTN. The sediment was re-dispersed to obtain FDTN-loaded nanoparticles, which were stocked by vacuum freeze-drying.

Considering tracking of drug-loaded nanoparticles, Coumarin-6 (Cou6), a classic model for studying drug tracking characteristics, was selected as an alternative to load nanoparticles (NP(C6)) by using the same method as FDTN-loaded nanoparticles.

2.7 Physicochemical characterization

The size, surface charge and size distribution of NPs were acquired by using a Malvern Zetasizer, Nano ZS, Malvern (USA). The structure and morphology were detected through a transmission electron microscope (TEM) (JEOL JEM1400 plus, Japan). The UV-vis absorption of NPs was measured by using a UV-vis spectrometer (Lambda 25, PerkinElmer, USA). The FTIR spectra were measured on KBr pressed pellet samples, in the range of 400-4000 cm^{-1} , with a VERTEX 70 spectrophotometer (Bruker, Germany).

The encapsulation efficiency (EE%) and loading efficiency (LE%) of FDTN loaded in Bio-PLGA-TK-PEG NPs were calculated as follows in a previous report.³⁰ The fresh purified NPs were prepared as described above. The supernatant was converged and the encapsulated cargo was determined by a UV-vis spectrometer (Lambda 25, PerkinElmer, USA). From the free drug available in the supernatant, the entrapped drug was

calculated and was expressed as loading efficiency. The EE and LE are expressed through the following formula:

$$EE\% = (\text{weight of loaded drug}) / (\text{weight of initially added drug}) \times 100;$$

$$LE\% = (\text{weight of loaded drug}) / (\text{total weight of Bio-PLGA-TK-PEG}) \times 100.$$

2.8 Synthesis Fc-functionalized nanoparticles

In order to prepare the Fc-functionalized nanoparticles, the storage nanoparticles, avidin and biotin-conjugated mouse/human IgG Fc fragment were mixed reaction according to a certain ratio.³¹ Briefly, two mg storage nanoparticles were dissolved in 250 μL PBS, then added 1,000 μL avidin (2 mg mL^{-1}), and gently stirred for 30 min at RT to allow avidin conjugation to the nanoparticles. The colloidal solution was washed three times with PBS by centrifugation (4 $^{\circ}\text{C}$, 12,000 rpm, 30 min) to remove the free avidin. The remaining nanoparticles were resuspended in 250 μL of water, and incubated with 1,000 μL biotin-conjugated mouse/human IgG Fc fragment (2 mg mL^{-1}) at RT under gentle stirring for 30 min. The product was washed three times with PBS by centrifugation (4 $^{\circ}\text{C}$, 12,000 rpm, 30 min) to remove unbound Fc. The sediment was re-dispersed to obtain Fc modified FDTN-loaded nanoparticles (NPs-FDTN), which were applied to the following test. To confirm the Fc were conjugated with NP, a certain NP(C6) and NP(C6)-Fc were dissolved in deionized water respectively, and made with the same fluorescence intensity ($F_{\lambda 466/504 \text{ nm}} = 152,000$). Then the conjugation of IgG Fc to the NP surface was measured with a protein bicinchoninic acid (BCA) assay.

2.9 In vitro stability of NPs-FDTN and drug release study

To assess the stability of NPs-FDTN, two mg of lyophilized sample was resuspended in 200 μL of PBS and 10% FBS, the size distribution of nanoparticles was acquired every 24 h for seven days at room temperature.

The drug release performance of NPs-FDTN (two mg of lyophilized sample was resuspended in 200 μL of PBS) was studied by using a dynamic dialysis method, under the circumstance of different concentrations of H_2O_2 (0 mM, 50 mM, 100 mM, and 200 mM) in vitro.^{30,32} The samples were placed into bag filters ($M_w = 10,000$) and immersed together into 4 mL PBS as the solution medium. Shaking at 37 $^{\circ}\text{C}$ and 100 rpm, the dialysate was obtained at a predetermined time point, and the drug release was recorded. Following, one mL of the solution was removed and replaced with an equal volume of fresh PBS. According to previous studies, UV-Vis absorption is a reliable method for detecting drug release. Therefore, the concentrations of drug in the sample solution were determined by UV-vis spectroscopy. The same amount of free drugs dissolved in PBS was measured as control and all trials were performed in triplicates.

To investigate whether NPs-FDTN promotes eosinophils apoptosis. The purified eosinophils were seeded in 100 μL medium (RPMI 1640 with 10% FBS) in 96-well cell plates (2×10^4 cell per well) and treated with NPs-FDTN at 3.5 $\mu\text{g L}^{-1}$ (equivalent to FDTN at 10.0 μM) at 37 $^{\circ}\text{C}$ in 5% CO_2 for 18 h. The early apoptosis (AnnV⁺/PI⁻) and late apoptosis (AnnV⁺/PI⁺) were detected by the flow cytometry (fluorescein isothiocyanate- Annexin V and PI).

2.10 Cellular uptake and intracellular tracking of Fc modified nanoparticles

16HBE cells were seeded in 24-well plates with slices at a density of 4×10^4 cells per well. NP(C6)-Fc 0.1 μg was added in every well at 80% confluence. After 2 h incubating, the cell climbing slices were gently washed and fixed with 4% paraformaldehyde, permeabilized, and stained intracellularly with nuclei (blue) and cytoskeletal proteins β -Actin (violet). To assess the cellular uptake and intracellular tracking of NP(C6)-Fc (green), the images were captured with the same imaging parameters by fluorescence microscopy.

To assess whether the Fc modified nanoparticles bypass lysosomes, the Nunc Lab-Tek II chamber slides (Thermo, USA) were pre-coated with 10% collagen in 0.02 M acetic acid solution 400 μL per well for 1h. The chambers were washed 2 times with PBS, and dried by air. LysoTracker[®] Red DND-99 (Invitrogen, USA) working medium was prepared with the NP(C6)-Fc 0.1 μg or NP(C6) 0.1 μg in RPMI 1640 medium at a final concentration of 100 nM. 16 HBE cells were seeded in Nunc Lab-Tek II chamber slides at a density

of 2×10^4 cells per well. When the cells were at 80% confluence, the cultural supernatant was discarded and washed gently, the working medium was then added to incubate for 2 h at 37 °C. The cells were gently washed 3 times with PBS, and stained for nuclei with DAPI (blue). The images of lysosomes in interaction with NP(C6)-Fc and NP(C6) were captured with the same imaging parameters by confocal microscopy.

2.11 Air-liquid interface (ALI) culture system for checking NPs across epithelial barrier

In vitro epithelial barrier model was established with Normal Human Bronchial Epithelial Cells (NHBEs) (CC-2540S, Lonza) and eosinophils were co-cultured upon an air-liquid interface (ALI) Pneuma Cult -Ex Culture System (Catalog #05050, Stem cell) according to manufacturer's specifications. Briefly, NHBEs at 5×10^4 cells in submerged culture for expansion are performed with Pneuma Cult-Ex Plus Medium. During the early ALI developmental stages, Pneuma Cult-Ex Plus was added to the apical and basal chambers. After 4 days, upon reaching the confluence, discarding the medium in both chambers, and Pneuma Cult-ALI-S was added to the basal chamber only. The culture lasted for 20 days. PBS, NPs and NPs-Fc were added in the apical chambers respectively, Eos at 10×10^4 cells in 1mL were added in the basal chambers. After 12 h culture, the filter membranes were made into slices and measured through the Jeol Jem 1400 transmission electron microscope.

2.12 Induction of eosinophilic allergic airway inflammation

Female BALB/c mice, 8-week-old (18-20 g), were obtained from Guangdong Medical Laboratory Animal Center. They were randomly housed in individual cages (5 per cage) under the conditions of temperature (25 degC), air humidity (50%) and specific pathogen-free conditions, and maintained on a 12h light/dark cycle with free access to food and water. Before the treatment, the mice were habituated to the environment for one week. The present experimental procedure was approved by the Institutional Animal Care and Use Committee of the Second Affiliated Hospital of Guangzhou Medical University (Approval No. A2019-048).

The mice were immunized through intraperitoneal injections of 20 μ g of chicken ovalbumin (OVA) emulsified in alum (2.25 mg of $\text{Al}(\text{OH})_3$ per 2 mg of $\text{Mg}(\text{OH})_2$) in 100 μ L PBS on days 0 and 14. The mice were challenged with a 1% OVA in saline for 40 min by means of ultrasonic nebulization on consecutive days 24, 25, and 26. The mice were randomly divided into five groups (5 mice per group) including FDTN, NPs-FDTN, BUD, models groups and negative control groups. Two hours after each OVA challenge, with the achievement of anesthesia, mice in the FDTN group were treated by means of intratracheal administration of 50 μ L of FDTN (1.2 mg mL^{-1})¹⁸, mice in the NPs-FDTN group were treated intratracheally administration of 50 μ L of NPs-FDTN (7.5 mg mL^{-1} , equivalent to FDTN at 10.0 μ M according to FDTN LE% of nanoparticles), mice in the BUD group were treated by means of intratracheal administration of 50 μ L of BUD (0.24 mg mL^{-1})³³. Three days later, on day 29, the airway hyperresponsiveness (AHR) to gradient concentrations of methacholine (Mch) (0, 3.125, 6.25, 12.5, 25, 50 mg mL^{-1}) was recorded with the Whole-body Plethysmograph System (Buxco® FinePointe™, USA). Then, all mice were sacrificed for analysis. The blood was collected via excising their eyeballs, and the serum was stored at -80 °C. Bronchoalveolar lavage (BAL) fluid was obtained by flushing the lungs with 0.7 mL PBS three times via tracheal cannula, and stored on ice. The left lungs, heart, liver, spleen and kidney were fixed in 4% paraformaldehyde (Sigma), the right lungs were kept in medium on ice for the subsequent processing.

2.13 Immunofluorescence

To assess our nanoparticles targeting FcRn in the lung, a certain NP(C6) and NP(C6)-Fc working solution was prepared in deionized water respectively, and made them with the same fluorescence intensity ($F_{\lambda 466/504\mu} = 152.000$). Every wild-type mouse was treated by means of intratracheal administration of 50 μ L of NP(C6) or NP(C6)-Fc. One hour later, the mice were anesthesia, their eyeballs were bled and the lung tissue sections were frozen in Tissue-Tek OCT on drikold. The frozen tissues were cut into cross sections with a thickness of 12 μ m. The sections were fixed in an oven at 37 °C for 30 min, and then blocked with 10% goat serum for 1 hour. The samples were incubated with anti-mouse FcRn IgG (R&D Systems) overnight and then incubated with Goat IgG (H+L) APC-conjugated antibody (R&D Systems), developed with DAPI. Fluorescent images were obtained with the Zeiss LSM 880 scanning confocal microscope.

2.14 In vivo fluorescence imaging

To assess the nanoparticles uptake, transepithelial transport in the airway and residence time in the lung, the eosinophilic allergic airway inflammation model mice were established by using the same method as above. A certain NP(C6) and NP(C6)-Fc working solution was prepared in deionized water respectively, and made with the same fluorescence intensity ($F_{\lambda 466/504\text{nm}} = 152.000$). Every mouse was treated by means of intratracheal administration of $50\mu\text{L}$ of NP(C6) or NP(C6)-Fc. After anesthesia, the eyeballs were bled and the lungs were taken at different time points (0, 2, 4, 8, 12, 24, 48 h) from day 27 (**Figure 5B**). The lung tissue sections were frozen in Tissue-Tek OCT on drikold. The frozen cross sections with a thickness of $12\mu\text{m}$ were immediately measured by fluorescence microscopy. Average fluorescence intensity was detected by Image J software.

2.15 Bronchoalveolar lavage fluid

The total cell counts were examined by the automatic modular blood and body fluid analyzer (Sysmex XN 2000, Japan) according to the standard operating procedures of the laboratory. BAL cells were stained with anti-CD45 (30-F11), anti-CD11b (M1/70), anti-CD11c (HL3), anti-Ly6G (1A8), anti-Siglec-F (E50-2440) and Fixable Viability Stain 510 according to the manufacturer's specifications. Cells were then analyzed by flow cytometry.

2.16 Pathological examination of lung tissues

The overnight fixed lungs with 4% paraformaldehyde (Sigma) were embedded in paraffin and made into pathologic slides ($4\mu\text{m}$) for hematoxylin and eosin (H&E) or periodic acid-Schiff (PAS) staining. To quantify airway inflammation, a histological scoring system⁷ was applied as the following scale, with the mean value taken: 0 = normal, no inflammation cell was detectable; 1 = occasional inflammatory cell accumulation; 2 = most bronchi or vessels surrounded by one layer (1 to 10 cells) of inflammatory cells; 3 = most bronchi or vessels were surrounded by 2 layers (10 to 20 cells) of inflammatory cells; 4 = most bronchi or vessels were surrounded by more than two layers (more than 20 cells) of inflammatory cells. On the other hand, the percentage of PAS positive goblet cells of the total epithelial cells around airways was counted to quantify mucus production.

2.17 Flow cytometric analyses of lung cells

The right lung was thoroughly minced with scissors on ice, and transferred into RPMI 1640 medium containing collagenase (200 U mL^{-1} , Gibco® Life Technologies) and deoxyribonuclease I ($200\mu\text{g mL}^{-1}$, Gibco® Life Technologies) for enzymatical digestion for 30 min at $37\text{ }^\circ\text{C}$. The digestion solution was filtered with a $40\mu\text{m}$ mesh, and red blood cells were lysed by lysing solution (BD FACS). The single-cell suspension was then divided into two equal parts. One part was used to extracellular staining with anti-CD45 (30-F11), anti-CD11b (M1/70), anti-CD11c (HL3), anti-Ly6G (1A8), anti-Siglec-F (E50-2440) and Fixable Viability Stain 510 according to the manufacturer. The other part was applied to intracellular staining. The cells were ex vivo stimulated with PMA (10 ng mL^{-1} , Sigma) and Ionomycin ($1\mu\text{M}$, Sigma) for 5 h, and the monensin ($2\mu\text{M}$, Sigma) was added during the last 3 h of stimulation. The cells were washed and resuspended for extracellular staining with anti-CD45 (30-F11), anti-CD3e (145-2C11), anti-CD4 (R4-5). Then, cells were immediately fixed with 4% paraformaldehyde, permeabilized, and stained intracellularly with anti-IL-4 (11B11), anti-IL-5 (TRFK5), anti-IL-10 (JES3-9D7), anti-IL-13 (eBio13A), anti-IL-17A (TC11-18H11), anti-IFN γ (XMG1.2). The single cells were then analyzed by flow cytometry.

2.18 Serological test

The serum stored at $-80\text{ }^\circ\text{C}$ was placed at room temperature for 30 min so that the frozen samples were completely thawed. The activity of alanine aminotransferase (ALT), and aspartate aminotransferase (AST), and the concentrations of creatinine (CREA) of serum were measured by an automatic biochemical analyzer (Cobas®8000 Automatic biochemical analyzer) according to the laboratory standard operating procedures. Among them, ALT and AST were applied to assess liver function, CREA was used to assess kidney

function. The total serum IgE levels were analyzed through an ELISA kit according to the manufacturer’s specifications.

2.19 Toxicity of FDTN, NPs-FDTN and BUD in vivo

The overnight fixed mice heart, spleen and kidney with 4% paraformaldehyde (Sigma) were embedded in paraffin and made into pathologic slides (4 μm) for hematoxylin and eosin (H&E), the images were gotten by Automatic digital slide scanning system (PRECICE500B, Beijing China).

2.20 Statistical analysis

All data are presented as the means \pm standard deviation (SD) as indicated. Statistical significance was determined by a two-tailed Student’s t-test ($\alpha = 0.05$) assuming equal variance. Statistical differences were analyzed by the GraphPad Prism 8 software.

3. Results

3.1 FDTN induces apoptosis of human eosinophils in a concentration-dependent manner

As the prolonged eosinophil survival plays a causal role in the asthma pathogenesis, we assessed the apoptosis-inducing potential of the JAK2 inhibitor FDTN (Figure S1) in human eosinophils. Peripheral blood eosinophils from asthma patients were incubated for 18 h with either the vehicle medium or increasing concentrations of FDTN. FDTN induced apoptosis in a dose-dependent fashion (Figure 1A, B). The proportion of early apoptotic cells (Annexin V⁺/PI⁻) increased along with the increasing concentrations of FDTN, and FDTN at 10.0 μM induced the late stage apoptosis in eosinophils (Annexin V⁺/PI⁺). The eosinophil viability was high ($95.8 \pm 0.7\%$) in the presence of IL-5 after 18 h, which was significantly reduced by FDTN, with the survival rate to $16.6 \pm 7.4\%$ at 10 μM FDTN (Figure 1C). During apoptosis the lactate dehydrogenase (LDH) in the cytoplasm will be released due to the membrane damage³⁴. Indeed, FDTN (10.0 μM) induced significantly more LDH than that the vehicle group did (Figure 1D). Transmission electron microscopy (TEM) and light microscopy data showed that FDTN-treated eosinophils displayed the typical morphological characteristics of apoptosis (Figure 1E, F). The control eosinophils were round with smooth cell surface and few microvilli. The nucleus with two lobules showed a high concentration of heterochromatin and the cytoplasm contained numerous eosinophilic granules. In contrast, the FDTN-treated eosinophils showed cellular shrinkage, nuclear condensation, and chromatin condensation along the nuclear membrane. Wright staining showed that the control eosinophil cytoplasm was filled with thick, neat, uniform, tightly arranged orange-red eosinophilic granules. Most cells had two lobules and were dark purple. Consistent with the TEM data, the FDTN-treated eosinophils showed the typical apoptotic characteristics (cellular shrinkage and nuclear condensation) (Figure 1F). These data demonstrated that FDTN induced apoptosis of eosinophils in a dose-dependent manner.

3.2 FDTN inducesthe cell-intrinsic apoptosis pathway in human eosinophils

We first assessed the effect of FDTN on the STAT phosphorylation levels by flow cytometry and western blot. FDTN decreased JAK2, p-JAK2, STAT5 and p-STAT5 levels dose-dependently (Figure 2A, B and C) without affecting the p-STAT3 and p-STAT6 levels (Figure S2). We next investigated if FDTN activated the apoptotic pathway. FDTN increased the cleaved caspase-3 level in a dose-dependent manner (Figure 2D, E and F). The pro-apoptosis regulator Bad is normally localized in the cytoplasm but rapidly migrates to the mitochondria when the apoptotic signal is received.^{35,36} Figure 2G shows that the colocalization (orange-yellow color) between BAD and mitochondria in FDTN- treated eosinophils, but it could hardly be seen in the control cells. Thus, these results suggest that FDTN induced the apoptotic pathway by blocking the JAK2/STAT5 pathway, which was contributed to not only general cytotoxicity, but also intrinsic pathway of apoptosis.

3.3 Preparation and characterization of NPs-FDTN

In order to protect FDTN from random simple diffusion and from being degraded in the transportation process, the NPs-FDTN were synthesized and purified as described in the method section. The TEM images

show the blank and NPs-FDTN had a smooth surface and a circular shape (Figure 3A, C). The Nanoparticle Tracking Analysis (NTA) was used to evaluate the size distribution of blank nanoparticles (NPs) and NPs-FDTN. The data showed that the peak value of size was < 100 nm, and the average diameters of the blank and FDTN-loaded NPs were 68 nm and 98 nm, respectively (Figure 3B, D). The particle size of NPs-FDTN in the TEM image was slightly smaller than that measured by NTA due to the hydration shell. In addition, the zeta potentials of the blank and drug-loaded NPs were 25.4 mV and 37.0 mV, respectively (Figure 3H), suggesting that nanoparticles are much likely to interact with the negatively charged cell surfaces. The encapsulation efficiency (EE%) and loading efficiency (LE%) of nanoparticles for drugs were 83.6% and 16.0%, respectively. The UV-vis spectra of free FDTN, NPs-Blank and NPs-FDTN in aqueous solution showed that the free FDTN had a specific absorption peak at 268 nm, which was observed in NPs-FDTN but not in NPs-Blank (Figure 3E). This confirmed that FDTN had been loaded into the nanoparticles and that the emulsification process did not change the chemical structure of the loaded FDTN.

The FTIR spectra of free FDTN, NPs-Blank and NPs-FDTN are shown in Figure 3F. The spectra of FDTN shows free hydroxyl at 3352 cm^{-1} ; specific -NH-bond at 2968 cm^{-1} ; CH ring stretching vibration at 1500 cm^{-1} ; -SO bond at 796 cm^{-1} . The spectra of NPs-Blank shows -OH bond at 3424 cm^{-1} ; -CH₂-bond at 2943 cm^{-1} ; specific -CO bond at 1756 cm^{-1} ; -C-O-C bond at 1096 cm^{-1} . Compared with NPs-Blank, NPs-FDTN had -OH bond at 3424 cm^{-1} ; -CH₂- bond at 2943 cm^{-1} ; specific -CO bond at 1756 cm^{-1} ; -COC- bond at 1096 cm^{-1} . In particular, the aromatic hydrocarbons at 785 cm^{-1} out-of-plane bending vibration (four adjacent hydrogens) indicated that FDTN is covalently attached to PEG-TK-PLGA and encapsulated in nanoparticles. In addition, the size of the NPs remained around 100 nm with little fluctuation in PBS/10% FBS for seven days (Figure 3G), indicating its good stability.

3.4 Biological availability assessment of nanoparticles

Our synthetic nanomaterials are embedded with a ROS-cleavable thioketal (TK) cross-linker.³⁷ PEG-TK-PLGA polyplexes are fractured in a ROS-rich microenvironment (Figure 4A). Indeed, TEM images show that NPs were spherical and uniform in the absence of H₂O₂ but got fractured after 12 h in 50 mM H₂O₂ (Figure 4E). The cumulative amount of free FDTN ($\sim 45\%$) within 108 h was significantly higher than that of the original free FDTN ($\sim 3\%$) (Figure 4 F), indicating a sustained drug release. The release of FDTN by the nanoparticles was fully dependent on the ROS concentration. Then, we cultured the eosinophils with NP-FDTN at $3.5\ \mu\text{g L}^{-1}$ (equivalent to FDTN at $10.0\ \mu\text{M}$). NPs-FDTN induced the early and late stage apoptosis in eosinophils, and NPs-Blank had no toxicity to eosinophils (Figure 4C, D).

In order to deliver nanoparticles via FcRn-mediated transcytosis, we modified nanomaterials with Fc by the avidin-biotin interaction. The bicinchoninic acid (BCA) assay result (Figure S4B) showed that the protein concentration of NP(C6)-Fc was more than twice that of NP(C6), indicating the conjugation of IgG Fc to the NP surface. Figure 4B shows that nanomaterials modified with Fc didn't go through the endocytosis and lysosomal degradation. The TEM image shows FDTN-loaded nanoparticles modified with Fc had a smooth surface and a sphere shape, and the size of nanoparticles was < 100 nm (Figure S4A). To track the NPs inside the cells, we loaded NP(C6)-Fc with coumarin 6 (Cou6, green fluorescent dye) and modified with Fc. NP(C6)-Fc was added to the human airway epithelial cell line 16HBE cells and localization was analyzed by fluorescence and confocal microscopy. NP(C6)-Fc was readily taken up and localized mainly in the cytoplasm (Figure 4G), but not in the lysosome as it was not co-localized with the lysosomal marker Lysotracker® Red (Figure 4H). Fc-modified NPs taken up by a monolayer of the normal human bronchial epithelial cell line NHBE was confirmed by TEM (Figure S6). Thus, our NP(C6)-Fc strategies possess high ROS-responsiveness, and can be easily taken up by epithelial cells and bypass the lysosomes.

3.5 In vivo transepithelial transport

The airway epithelial cells and their tight junctions form a strong natural biological barrier, which restricts the transportation of different substances including drugs (Figure S6). We next investigated whether NP(C6)-Fc crossed the airway epithelial barrier via FcRn in the mouse lung. NP(C6) or NP(C6)-Fc were administered i.t. to wild-type (WT) mice, and the lungs were harvested for sectioning and imaging 1 h

later. The immunofluorescence result showed that FcRn was localized to the airway epithelium (Figure 5A). C6 loaded NP(C6)-Fc (green) was detected throughout the lung parenchyma but little NP(C6) signal was seen, and NP(C6)-Fc was co-localized with FcRn (Figure 5A). The OVA-challenged mice (on day 27) were injected i.t. with either NP(C6) or NP(C6)-Fc and the frozen lung sections were prepared at the indicated time points to track the NPs (Figure 5B). Right after injection, a similar amount of NP(C6) and NP(C6)-Fc were detected around the airway lumen. However, little NP(C6) signal was seen 4 h after injection, whereas in NP(C6)-Fc was still detected not only in the airway lumen but also in the lung parenchyma up to 48 h (Figure 5E, F). The fluorescence intensity of NP(C6)-Fc treated group was significantly higher than that of NP(C6) treated group (Figure 5C). Also, in NP(C6)-Fc treated group, though the fluorescence intensity dropped gradually, a relatively low and stable level of fluorescence persisted (Figure 5D, F). These results demonstrated Fc-modified nanoparticles can be directed to FcRn and cross the transepithelial barrier into the lung parenchyma like the soldiers tactfully hiding in Trojan horse, and that Fc-conjugation can significantly prolong their residence time in the lung.

3.6 NPs-FDTN ameliorate allergic airway inflammation significantly better than free FDTN

Having demonstrated the bio-availability of NPs-FDTN in mouse lung, we next investigated whether NPs-FDTN could attenuate eosinophilic airway inflammation better than free FDTN. We compared the effect of FDTN, NPs-FDTN, and the corticosteroid budesonide (BUD) in the eosinophilic airway inflammation model³⁸ (Figure 6A). H&E staining (Figure 6B) and the inflammatory scores (Figure 6E) showed that infiltrating immune cells were significantly increased in model group, and were notably decreased in the NPs-FDTN and BUD groups, but not in FDTN group ($p = 0.079$). PAS staining (Figure 6B, F) showed that all three treatments significantly decreased the mucus production by goblet cells. All three treatments considerably decreased airway resistance at 50 mg mL⁻¹ of methacholine (Mch) (Figure 6C), NPs-FDTN group exhibited a clear declining trend via FDTN group, but there was no significant difference among the three treatments. The serum IgE levels were substantially decreased in the NPs-FDTN and BUD groups, but not in the FDTN group (Figure 6D). These results altogether demonstrated that FDTN-NPs have therapeutic advantages over free FDTN.

3.7 NPs-FDTN suppress the immune response significantly better than free FDTN

To further assess the effects of FDTN and NPs-FDTN on inflammatory cells and inflammatory cytokine levels in vivo, the bronchoalveolar lavage (BAL) fluid was analyzed. The gating strategy for flow cytometry is shown in Figure S7. In the OVA control group, more than 90% of infiltrating cells were eosinophils (SiglecF⁺, Ly6G⁻) within the gate of CD45⁺CD11c⁻CD11b⁺ cells, with no more than 1% neutrophils (Figure 7A), which indicating that the eosinophilic asthma model was successfully established. FDTN, NPs-FDTN, and BUD all significantly decreased the total cell numbers compared to the OVA control (Figure 7B). The BUD group had the greatest reduction and the NPs-FDTN group was significantly better than FDTN group. NPs-FDTN and BUD, but not FDTN, significantly reduced the neutrophil infiltration (Figure 7C). The number of eosinophils was decreased by FDTN, NPs-FDTN and BUD, and the trend was similar to the total cell counts. Interestingly, the NPs-FDTN group and BUD group were significantly more improved than that in the FDTN group, and there was no significant difference between the NPs-FDTN group and BUD group in the eosinophil counts (Figure 7D).

We next assessed inflammatory cells and cytokines in the lung tissues. The numbers of eosinophils and CD4⁺ T cells were significantly reduced by NPs-FDTN and BUD groups, but not by FDTN (Figure 7E, F). Expression of cytokines were significantly decreased by all three therapy strategies (Figure 7G). However, NPs-FDTN was far superior to FDTN in suppression of cytokines such as IL-4, IL-5 and IFN- γ . In all, just like amelioration allergic airway inflammation, NPs-FDTN suppress the immune response significantly better than free FDTN.

While FDTN and NPs-FDTN had no effects on the liver function, BUD significantly increased the serum activity of ALT and AST (Figure 7H, I and S9). Consistently, H&E staining showed edema in the liver treated with BUD, but not with FDTN or NPs-FDTN. However, no obvious damages were found in the heart, spleen

or kidney in three treatment groups (Figure S9). These results indicated that while three therapy strategies have anti-inflammatory effects, NPs-FDTN were better than FDTN and similar to budesonide but with less side effects.

4. Discussion

The cytokine-mediated signals are primarily transduced by the JAK/STAT signaling cascade, and JAK2 is an important mediator in the fate of immune cells.³⁹⁻⁴¹ In this study, we selected FDTN, a selective JAK2 inhibitor, to treat allergic asthma. Our data showed that FDTN induced apoptosis of eosinophils in a concentration-dependent manner. JAKs are a family of non-receptor tyrosine kinases, including JAK1, JAK2, JAK3, and Tyk2. When extracellular cytokines bind to their corresponding receptors on the cell membrane, the receptors are dimerized and sequentially activate JAK tyrosine kinases. Then, specific tyrosine residues on the tails of receptors in cytoplasmic are phosphorylated by activated JAKs. These phosphorylated specific tyrosine residues provide docking sites to STATs. Subsequently, STATs are phosphorylated and formed dimer. The dimers translocate to the nucleus and regulate gene expression.¹¹ Based on the mechanism of JAK/STAT pathway, that FDTN promoted eosinophils apoptosis is much likely due to the regulations of intracellular apoptosis-related proteins. In agreement with the hypothesis, our results showed that the treated eosinophils JAK2, p-JAK2, STAT5 and p-STAT5 levels were inhibited in dose-dependent, the pro-apoptosis Bad protein migrated from cytoplasm to the mitochondria, cleaved caspase-3 was markedly increased in dose-dependent. Meanwhile, LDH released by eosinophils increased significantly. Previous studies have demonstrated that JAK2/STAT5 upregulated the expression of Bcl-xL to enhance cell survival.⁴² In turn, BAD can interact with Bcl-2 or Bcl-XL with BH3-only proteins, and prevent Bcl-2 or Bcl-XL from binding to the Bax-like proteins, which have proapoptotic effect.³⁵ Thus, FDTN inhibited the JAK2/STAT5 pathway related to cytokines activating eosinophils, and in turn, inhibited eosinophils proliferation and induced eosinophils apoptosis. That FDTN induced eosinophil apoptosis was ascribable to not just general cytotoxicity, but intrinsic pathway of apoptosis.

In patients with Type-2 asthma, Th2 cells and other innate immune cells produce Th2-cell-associated cytokines, those cytokines in turn promote pathological damages underlying airway obstruction. All these changes further lead to the vicious cycle in the pathogenesis of asthma.^{43,44} In our study, using OVA/alum-induced inflammation model recently reported³⁸, we established eosinophilic asthma model. The eosinophilic asthma mice were treated by FDTN intratracheal administration, not only the numbers of eosinophils etc. inflammatory cells in BAL fluid and lung tissue, but also inflammatory cytokines level (IL-4, IL-5, IL-13, IL-10, IL-17A and IFN γ) in lung tissue were significantly decreased. These results demonstrated that FDTN had efficacy of improve asthma inflammation. Some asthma-relevant cytokines receptors, such as the receptors of GM-CSF, IL-3, IL-5, IL-6, IL-13, IFN γ and TSLP share the common β -chain except each unique α -chains.^{17,45,46} There are multiple tyrosine residues in β -chain, which serves as substrate of JAK2. These tyrosine residues are phosphorylated by JAK2 and active the downstream of the signaling pathway.⁴⁵ The JAK/STAT signal pathway serves as a bridge to communicate these cytokines with the pathological changes such as airway hyperresponsiveness, mucus production, immunoglobulin class switching, and eosinophil recruitment and survival.^{12,47,48} So, inhibition of JAK2 means blocking the common β -chain, and results in cytokines effects suppression. JAK2-inhibited or deficient cells failed to respond to IL-3, GM-CSF, IFN- γ , and TSLP⁴⁹⁻⁵¹. JAK inhibitor were used as not only research tools but also clinical treatments. For example AG490, a well-established Jak2 inhibitor was used to treat polymicrobial sepsis⁵². FDTN was explored to treat myelofibrosis as an oral selective JAK2 inhibitor¹⁹. FDTN is an anilinoimidazole derivative and selectively inhibits JAK2 in low concentration. Here, we utilized FDTN as asthma treatment by means of its inhibition properties of JAK2. The results suggested that FDTN have significant therapeutic efficacy not only in pro-apoptosis intrinsic of eosinophils, but also in limiting infiltrating immune cells and improving pathological injury, which may due to FDTN inhibited the JAK/STAT signal pathway and weakened the communication between cytokines and effector cells in inflammatory microenvironment. Thus, blocking a common intracellular signal transduction may provide more efficacious therapeutic strategy rather than individual cytokine or receptor.

A key factor of asthma treatment is to deliver the drugs to the lung tissue. The airway epithelial cells and tight junction of each other form a compact natural biological barrier, which controls the transportation of different substances (Figure S6). This natural barrier is the first challenge of intratracheal administration. The molecular weight of pharmaceuticals is very important. The macromolecules have difficulty in crossing the cell membrane and tight junction. Although the micromolecules can be easily penetrated into cells by simple diffusion and even access cell organelles, they show off-target effects and decrease bioavailability, even increase systemic side effects.⁵³ In present study, FDTN was lipid solubility, and the molecular weight was 524.68. That FDTN was directly administrated intratracheally also had to suffer the hindrance of airway barrier and face simple diffusion for lipid solubility and small molecule. These may lead to low bioavailability. It's not hard to see from our results that the extents of improvement of FDTN attenuated the airway inflammation were obvious inferior to budesonide. In order to improve bioavailability and therapeutic efficacy of FDTN, nano-material technology was introduced in this study.

In our study, the ROS responsive PEG-TK-PLGA block polymer and FDTN were assembled into nanoparticles through ultrasonic emulsification, subsequently, the nanoparticles were modified with Fc portion of IgG by means of avidin-biotin system. The efficacy of NPs-FDTN in treatment eosinophilic asthma was assessed through comparison of free FDTN and BUD. The results demonstrated that NPs-FDTN had more advantages than free FDTN in attenuation the number of inflammatory cells and inflammatory cytokines levels, limitation of infiltrating immune cells around bronchial regions and mucus producing by goblet cells, improvement of bronchial hyper-reactivity and switching total serum IgE levels. Even in BAL fluid eosinophils, lung eosinophils, lung CD4⁺ cells, lung IL-5, IL-13 and so on lung cytokines, there were not significant difference between NPs and BUD. The therapeutic efficacy of FDTN was significantly increased by application of nano-material technology.

In recent decade, PLGA-PEG copolymers have been widely applied in pharmaceutical products and drug delivery systems.⁵⁴ PLGA-PEG copolymer is an amphiphilic polymer assembled by PLGA and PEG, and possess the advantages of both the biodegradability and biocompatibility of PLGA and PEG. The hydrophobic PLGA inside the micelles can entrap the hydrophobic drugs, and the hydrophilic PEG outside the micelles can maintain a stabilizing shell and provide some chances to bind extra groups.⁵⁵ Our results showed that the encapsulation efficiency (EE%) and loading efficiency (LE%) of nanoparticles for drugs was as high as 83.6% and 16.0%, respectively. Hydrophobic FDTN was assembled inside the micelles, which was favor of avoiding random simple diffusion and being degraded in the transportation process.

Secondly, our nanoparticles were modified with Fc portion of IgG. Fc is the ligand of the neonatal Fc receptor (FcRn). FcRn was early found existing in the apical region of small intestine epithelial cells, and diffusely throughout the colon from fetuses to adults. FcRn-dependent pathway of transcytosis diverts IgG crossing epithelial barrier away from degradation in the lysosomes and protect IgG from intracellular catabolism.⁵⁶ The IgG/FcRn transcytosis pathway was applied in transepithelial transport of nanoparticles.^{57,58} Adult human and mouse lung bronchial epithelial cells also expressed FcRn,²⁷ in such studies, through Fc-mediated transport, nanoparticles could across airway epithelial cell layers,⁵⁷ and erythropoietin Fc fusion protein crossed the epithelial barrier and kept intact and fully functional.⁵⁹ Consistent with a FcRn-mediated pathway of transcytosis, the present results demonstrated that our NPs could be easily uptake by 16HBE cells and bypassed the lysosome, and more efficiently transported from airway to lung tissues. More importantly, the immunofluorescence result showed that our NPs was co-localized with FcRn expressing on airway epithelial cells, and the eosinophilic airway inflammation model mice lung frozen sections showed that the nanoparticles modified with Fc could be transepithelial transport and resident in lung parenchyma for a longer time, which means that drugs have more chance to act on inflammation microenvironment. Thus, based on Fc/FcRn-mediated transcytosis, FDTN was brought into the lung tissues with good quality and quantity just liked tactfully hiding in Trojan horse.

Recently, various smart polymers responded to ROS were designed to deliver the pharmaceuticals in tumor environment for cancer targeting treatment.⁶⁰ During asthma, there is a high level of ROS in the airway microenvironment,^{28,29} our synthetic nanomaterials were embedded thioketal (TK), which served as a ROS

senser, could be cleaved by ROS.³⁷ The destabilization of TEM was visual to display that the spherical particles turned into linear in the absence of H₂O₂. The quantity data also indicated the release of FDTN from the nanoparticles was increased along with time and increasing levels of H₂O₂. Thus, When the NPs were delivered into ROS microenvironment, TK was cleaved, and the PEG-TK-PLGA polyplexes was fractured, then FDTN inside was released. In addition, the nanoparticle size is an important character. nanoparticles were easy to deposit in the smaller airways and reside in the lung tissues for a long time.⁶¹ Our nanoparticles average size was approximately 100 nm, this size may be more suitable for enhancing retention in lung. The longer time the FDTN loaded NPs resided in the lung tissues, the more sustainable release of FDTN from NPs cleaved by ROS. The synthetic materials PEG and PLGA are FDA approved biodegradable materials, it made no influence to cell viability and any injury to liver and kidney. Interestingly, budesonide (BUD), as a clinical routine medication, showed liver injury in this mice experiment, which further highlighted the advantages of nanomaterials.

5. Conclusions

In conclusion, our findings showed that FDTN, a JAK2 inhibitor, induces apoptosis of eosinophils via inhibition of the JAK2/STAT5 signaling pathway in vitro and has significant therapeutic efficacy in limiting infiltrating immune cells, diminishing inflammatory cytokines level and ameliorating pathologic injury in the lung of eosinophilic airway inflammation model mice. The synthesized FcRn-targeting, ROS-responsive and FDTN-caged nanoparticles can bypass the lysosomes and overcome the airway epithelial barrier into the lung parenchyma with a long residence time, which vastly improve the therapeutic efficacy of free FDTN. This thesis creatively proposes combining the JAK2 inhibitor and nanoparticle technology as a treatment of eosinophilic airway inflammation. It provides a reference for the follow-up development of the cross-disciplinary application in the treatment of diseases.

Funding

This research was funded by the National Natural Science Foundation of China (Nos. 81871266, 51933011) and Scientific and Technological Projects of Guangzhou (No. 201804020042).

Acknowledgments

We thank Professor Jongdae LEE at Guangzhou Medical University for critical reading and scientific discussion.

Conflict of Interest

The authors declare no conflict of interest.

References

1. Masoli M, Fabian D, Holt S, Beasley R, Global Initiative for Asthma P. The global burden of asthma: executive summary of the GINA Dissemination Committee report. *Allergy*. 2004;59(5):469-478.
2. Lambrecht BN, Hammad H. The immunology of asthma. *Nat Immunol*.2015;16(1):45-56.
3. Hammad H, Lambrecht BN. The basic immunology of asthma. *Cell*.2021;184(6):1469-1485.
4. Lee JJ, Dimina D, Macias MP, et al. <6-Defining a Link with Asthma in Mice Congenitally Deficient in Eosinophils.pdf>. *Science*. 2004;305(5691):1773-1776.
5. Humbles AA, Lloyd CM, McMillan SJ, et al. A critical role for eosinophils in allergic airways remodeling. *Science*.2004;305(5691):1776-1779.
6. Grozdanovic M, Laffey KG, Abdelkarim H, et al. Novel peptide nanoparticle-biased antagonist of CCR3 blocks eosinophil recruitment and airway hyperresponsiveness. *J Allergy Clin Immunol*.2019;143(2):669-680 e612.

7. Lucas CD, Dorward DA, Sharma S, et al. Wogonin induces eosinophil apoptosis and attenuates allergic airway inflammation. *Am J Respir Crit Care Med.* 2015;191(6):626-636.
8. Fulkerson PC, Rothenberg ME. Targeting eosinophils in allergy, inflammation and beyond. *Nat Rev Drug Discov.* 2013;12(2):117-129.
9. Walsh GM. Eosinophil apoptosis and clearance in asthma. *J Cell Death.* 2013;6:17-25.
10. Pernis AB, Rothman PB. JAK-STAT signaling in asthma. *J Clin Invest.* 2002;109(10):1279-1283.
11. Shuai K, Liu B. Regulation of JAK-STAT signalling in the immune system. *Nat Rev Immunol.* 2003;3(11):900-911.
12. Kettle JG, Astrand A, Catley M, et al. Inhibitors of JAK-family kinases: an update on the patent literature 2013-2015, part 2. *Expert Opin Ther Pat.* 2017;27(2):145-161.
13. Nelson RK, Brickner H, Panwar B, et al. Human eosinophils express a distinct gene expression program in response to IL-3 compared with common β -chain cytokines IL-5 and GM-CSF. *The Journal of Immunology.* 2019;203(2):329-337.
14. He Y, Shi J, Nguyen QT, et al. Development of highly potent glucocorticoids for steroid-resistant severe asthma. *Proceedings of the National Academy of Sciences.* 2019;116(14):6932-6937.
15. Kelly EA, Esnault S, Liu LY, et al. Mepolizumab attenuates airway eosinophil numbers, but not their functional phenotype, in asthma. *Am J Respir Crit Care Med.* 2017;196(11):1385-1395.
16. Dougan M, Dranoff G, Dougan SK. GM-CSF, IL-3, and IL-5 Family of Cytokines: Regulators of Inflammation. *Immunity.* 2019;50(4):796-811.
17. Park YM, Bochner BS. Eosinophil survival and apoptosis in health and disease. *Allergy Asthma Immunol Res.* 2010;2(2):87-101.
18. Chen D, Zhang F, Wang J, et al. Biodegradable nanoparticles mediated co-delivery of erlotinib (ELTN) and fedratinib (FDTN) toward the treatment of eltn-resistant non-small cell lung cancer (NSCLC) via suppression of the JAK2/STAT3 signaling pathway. *Front Pharmacol.* 2018:1214.
19. Pardanani A, Harrison C, Cortes JE, et al. Safety and Efficacy of Fedratinib in Patients With Primary or Secondary Myelofibrosis: A Randomized Clinical Trial. *JAMA Oncol.* 2015;1(5):643-651.
20. Mei L, Zhang Z, Zhao L, et al. Pharmaceutical nanotechnology for oral delivery of anticancer drugs. *Adv Drug Deliv Rev.* 2013;65(6):880-890.
21. Omlor AJ, Le DD, Schlicker J, et al. Local effects on airway inflammation and systemic uptake of 5 nm PEGylated and citrated gold nanoparticles in asthmatic mice. *Small (Weinheim an der Bergstrasse, Germany).* 2017;13(10):1603070.
22. Gao GH, Park MJ, Li Y, et al. The use of pH-sensitive positively charged polymeric micelles for protein delivery. *Biomaterials.* 2012;33(35):9157-9164.
23. Wang Y, Xie H, Ying K, et al. Tuning the efficacy of esterase-activatable prodrug nanoparticles for the treatment of colorectal malignancies. *Biomaterials.* 2021;270:120705.
24. Wu H, Peng B, Mohammed FS, et al. Brain Targeting, Antioxidant Polymeric Nanoparticles for Stroke Drug Delivery and Therapy. *Small (Weinheim an der Bergstrasse, Germany).* 2022:2107126.
25. Qing G, Zhao X, Gong N, et al. Thermo-responsive triple-function nanotransporter for efficient chemophotothermal therapy of multidrug-resistant bacterial infection. *Nat Commun.* 2019;10(1):4336.
26. Martins JP, D'Auria R, Liu D, et al. Engineered Multifunctional Albumin-Decorated Porous Silicon Nanoparticles for FcRn Translocation of Insulin. *Small (Weinheim an der Bergstrasse, Germany).* 2018;14(27):1800462.

27. Sockolosky JT, Szoka FC. The neonatal Fc receptor, FcRn, as a target for drug delivery and therapy. *Adv Drug Deliv Rev.*2015;91:109-124.
28. MacPherson JC, Comhair SA, Erzurum SC, et al. Eosinophils are a major source of nitric oxide-derived oxidants in severe asthma: characterization of pathways available to eosinophils for generating reactive nitrogen species. *J Immunol.* 2001;166(9):5763-5772.
29. Sanders SP, Zweier JL, Harrison SJ, Trush MA, Rembish SJ, Liu MC. Spontaneous oxygen radical production at sites of antigen challenge in allergic subjects. *Am J Respir Crit Care Med.*1995;151(6):1725-1733.
30. Li G, Wang J, Xu M, et al. Engineered exosome for NIR-triggered drug delivery and superior synergistic chemo-phototherapy in a glioma model. *Applied Materials Today.* 2020;20.
31. Townsend SA, Evrony GD, Gu FX, Schulz MP, Brown Jr RH, Langer R. Tetanus toxin C fragment-conjugated nanoparticles for targeted drug delivery to neurons. *Biomaterials.* 2007;28(34):5176-5184.
32. Wang J, Li G, Tu C, et al. High-throughput single-cell analysis of exosome mediated dual drug delivery, in vivo fate and synergistic tumor therapy. *Nanoscale.* 2020;12(25):13742-13756.
33. Saglani S, Lui S, Ullmann N, et al. IL-33 promotes airway remodeling in pediatric patients with severe steroid-resistant asthma. *J Allergy Clin Immunol.* 2013;132(3):676-685. e613.
34. Goda T, Goto Y, Ishihara K. Cell-penetrating macromolecules: direct penetration of amphipathic phospholipid polymers across plasma membrane of living cells. *Biomaterials.* 2010;31(8):2380-2387.
35. Downward J. How BAD phosphorylation is good for survival. *Nat Cell Biol.* 1999;1(2):E33-35.
36. Jiang P, Du W, Heese K, Wu M. The Bad guy cooperates with good cop p53: Bad is transcriptionally up-regulated by p53 and forms a Bad/p53 complex at the mitochondria to induce apoptosis. *Mol Cell Biol.*2006;26(23):9071-9082.
37. Shim MS, Xia Y. A reactive oxygen species (ROS)-responsive polymer for safe, efficient, and targeted gene delivery in cancer cells. *Angew Chem Int Ed Engl.* 2013;52(27):6926-6929.
38. Tian BP, Xia LX, Bao ZQ, et al. Bcl-2 inhibitors reduce steroid-insensitive airway inflammation. *J Allergy Clin Immunol.*2017;140(2):418-430.
39. Yoshimura A, Ito M, Chikuma S, Akanuma T, Nakatsukasa H. Negative Regulation of Cytokine Signaling in Immunity. *Cold Spring Harb Perspect Biol.* 2018;10(7).
40. Seif F, Khoshmirasafa M, Aazami H, Mohsenzadegan M, Sedighi G, Bahar M. The role of JAK-STAT signaling pathway and its regulators in the fate of T helper cells. *Cell Commun Signal.* 2017;15(1):23.
41. O'Shea JJ, Plenge R. JAK and STAT signaling molecules in immunoregulation and immune-mediated disease. *Immunity.*2012;36(4):542-550.
42. Shen ZJ, Malter JS. Determinants of eosinophil survival and apoptotic cell death. *Apoptosis.* 2015;20(2):224-234.
43. Fahy JV. Type 2 inflammation in asthma—present in most, absent in many. *Nat Rev Immunol.* 2015;15(1):57-65.
44. Akdis CA, Arkwright PD, Bruggen MC, et al. Type 2 immunity in the skin and lungs. *Allergy.* 2020;75(7):1582-1605.
45. Geijsen N, Koenderman L, Coffey P. Specificity in cytokine signal transduction: lessons learned from the IL-3/IL-5/GM-CSF receptor family. *Cytokine Growth Factor Rev.* 2001;12(1):19-25.
46. O'Shea JJ, Schwartz DM, Villarino AV, Gadina M, McInnes IB, Laurence A. The JAK-STAT pathway: impact on human disease and therapeutic intervention. *Annu Rev Med.* 2015;66:311-328.

47. Jiang H, Harris MB, Rothman P. IL-4/IL-13 signaling beyond JAK/STAT. *J Allergy Clin Immunol.* 2000;105(6 Pt 1):1063-1070.
48. Zhong J, Sharma J, Raju R, et al. TSLP signaling pathway map: a platform for analysis of TSLP-mediated signaling. *Database (Oxford).* 2014;2014:bau007.
49. Parganas E, Wang D, Stravopodis D, et al. Jak2 Is Essential for Signaling through a Variety of Cytokine Receptors. *Cell.* 1998;93(3):385-395.
50. Neubauer H, Cumano A, Müller M, Wu H, Huffstadt U, Pfeffer K. Jak2 Deficiency Defines an Essential Developmental Checkpoint in Definitive Hematopoiesis. *Cell.* 1998;93(3):397-409.
51. Van Bodegom D, Zhong J, Kopp N, et al. Differences in signaling through the B-cell leukemia oncoprotein CRLF2 in response to TSLP and through mutant JAK2. *Blood.* 2012;120(14):2853-2863.
52. Pena G, Cai B, Deitch EA, Ulloa L. JAK2 inhibition prevents innate immune responses and rescues animals from sepsis. *J Mol Med (Berl).* 2010;88(8):851-859.
53. Mosquera J, Garcia I, Liz-Marzan LM. Cellular Uptake of Nanoparticles versus Small Molecules: A Matter of Size. *Acc Chem Res.* 2018;51(9):2305-2313.
54. Bouclier C, Moine L, Hillaireau H, et al. Physicochemical characteristics and preliminary in vivo biological evaluation of nanocapsules loaded with siRNA targeting estrogen receptor alpha. *Biomacromolecules.* 2008;9(10):2881-2890.
55. Locatelli E, Comes Franchini M. Biodegradable PLGA-b-PEG polymeric nanoparticles: synthesis, properties, and nanomedical applications as drug delivery system. *J Nanopart Res.* 2012;14(12).
56. Israel EJ, Taylor S, Wu Z, et al. Expression of the neonatal Fc receptor, FcRn, on human intestinal epithelial cells. *Immunology.* 1997;92(1):69-74.
57. Vllasaliu D, Alexander C, Garnett M, Eaton M, Stolnik S. Fc-mediated transport of nanoparticles across airway epithelial cell layers. *J Control Release.* 2012;158(3):479-486.
58. Yoshida M, Claypool SM, Wagner JS, et al. Human neonatal Fc receptor mediates transport of IgG into luminal secretions for delivery of antigens to mucosal dendritic cells. *Immunity.* 2004;20(6):769-783.
59. Bitonti AJ, Dumont JA, Low SC, et al. Pulmonary delivery of an erythropoietin Fc fusion protein in non-human primates through an immunoglobulin transport pathway. *Proc Natl Acad Sci U S A.* 2004;101(26):9763-9768.
60. Jager E, Hocherl A, Janouskova O, et al. Fluorescent boronate-based polymer nanoparticles with reactive oxygen species (ROS)-triggered cargo release for drug-delivery applications. *Nanoscale.* 2016;8(13):6958-6963.
61. Tian BP, Li F, Li R, et al. Nanoformulated ABT-199 to effectively target Bcl-2 at mitochondrial membrane alleviates airway inflammation by inducing apoptosis. *Biomaterials.* 2019;192:429-439.

Figure legends

Figure 1. FDTN induces apoptosis of human eosinophils in a concentration-dependent manner. **(A, B)** Apoptosis in eosinophils was determined by flow cytometry (n = 3). **(C)** Eosinophil viability was assessed by CCK8 assay (n = 3). **(D)** LDH activity in culture supernatant was detected by automatic biochemical analyzer (n = 3). **(E)** Eosinophil morphology was analyzed by Transmission electron microscopy (TEM) (Scale bar = 1 μ m), FDTN-treated eosinophils show cellular shrinkage, nuclear condensation, chromatin condensation and along the nuclear membrane. **(F)** Representative morphology of eosinophils by Wright staining ($\times 1,000$ original magnification). Black needle pointed to two eosinophils with the apoptotic morphology. Data were expressed as mean \pm SEM of individual groups of peripheral blood eosinophils from 3 asthma patients. (* $P < 0.05$, ** $P < 0.01$, and *** $P < 0.001$).

Figure 2. FDTN induces the intrinsic apoptosis pathway in human eosinophils. Peripheral blood eosinophils of asthma patients were isolated and incubated for 18h with either the vehicle or indicated amounts of FDTN. **(A)** Intracellular detection of p-SATA5 in eosinophils by flow cytometry. **(B)** The percentage of p-SATA5⁺ cells (n = 3). **(C)** Western blotting for JAK2 (125 kDa), STAT5 (90 kDa), p-STAT5 (90 kDa) and GAPDH (36 kDa). **(D)** Intracellular detection of cleaved caspase-3 in eosinophils by flow cytometry. **(E)** The cleaved caspase-3⁺ cell percentage (n = 3). **(F)** Western blotting for cleaved caspase-3 (17/19 kDa) and GAPDH (36 kDa). **(G)** The colocalization (orange-yellow color) of BAD (Red color) and mitochondria (Green color) was assessed by fluorescence microscopy (Scale bar: 10 μ m). Data were expressed as mean \pm SD of each group. (* P < 0.05, ** P < 0.01, and *** P < 0.001).

Figure 3. Characterization of nanoparticles. **(A, B)** TEM (Scale bar = 100 nm) image and size distribution of blank NPs. **(C, D)** TEM (Scale bar = 100 nm) image and size distribution of FDTN -loaded NPs. **(E)** The UV-vis spectra of free FDTN, NPs and NPs-FDTN in aqueous solution. **(F)** FTIR spectra of free FDTN, NPs and NPs-FDTN. **(G)** The stability of NPs in PBS/10% FBS. **(H)** The zeta potential of the NPs and NPs-FDTN.

Figure 4. Biological availability of NP-Fc. **(A)** Schematic illustration of drug release from NPs triggered by ROS. **(B)** Schematic illustration of NP-Fc uptake by 16HBE cells. **(C, D)** Apoptosis in eosinophils treated by NP-Fc was determined by flow cytometry (n = 3), Data were expressed as mean \pm SD (n = 3). (* P < 0.05, ** P < 0.01, and *** P < 0.001). **(E)** TEM (Scale bar = 100 nm) image of NPs in 50 mM H₂O₂ at 0 h and 12 h. **(F)** FDTN release from NPs at different concentrations of H₂O₂ (0, 50, 100, and 200 mM) for 108 h, and the drug release curve within 12 h. **(G)** Intracellular tracking of NP(C6)-Fc in 16HBE. Images were taken after incubation with NP(C6)-Fc for 2 h and observed by fluorescence microscopy (Scale bar = 10 μ m). NP(C6)-Fc (green), β -Actin (violet), nuclei (DAPI). **(H)** NP(C6)-Fc bypasses the lysosome assessed by confocal microscopy (Scale bar = 10 μ m). NP(C6)-Fc (green), β -Actin (violet), LysoTracker[®] (red), nuclei (DAPI).

Figure 5. FcRn-targeting, transepithelial transport and residence time of NPs in the lung of mice. **(A)** FcRn-targeting of NP(C6) and NP(C6)-Fc in the frozen lung section by confocal microscopy (Scale bar = 100 μ m). **(B)** Schematic illustration of NP(C6) and NP(C6)-Fc administration and lung sampling in the asthma model. **(C)** The comparative time-course fluorescence intensity between NP(C6) and NP(C6)-Fc. **(D)** The fluorescence intensity of NP(C6)-Fc in the lung sections at different time points. **(E)** Localization of NP(C6) and NP(C6)-Fc in the frozen lung section by fluorescence microscopy (Scale bar = 100 μ m) at different time. **(F)** Localization of NP(C6)-Fc in the frozen lung section by fluorescence microscopy (Scale bar = 100 μ m) at different time. Data were expressed as mean \pm SD (n = 3). (* P < 0.05, ** P < 0.01, and *** P < 0.001).

Figure 6. NPs-FDTN significantly attenuates the allergic airway inflammation. **(A)** Schematic illustration of the asthma model. **(B)** H&E- and PAS-stained lung sections (Scale bar = 100 μ m). **(C)** Airway hyper-responsiveness (AHR) measured with the Whole-body Plethysmograph System. **(D)** Serum IgE levels of different groups. **(E)** Inflammatory score of different groups. **(F)** PAS-stained cells per bronchi (%) of different groups. Data are expressed as the mean \pm SD of individual groups of mice (n = 5 mice per group; * P < 0.05, ** P < 0.01, and *** P < 0.001, NS, not significant).

Figure 7. NPs-FDTN attenuate the immune response better than FDTN. **(A)** Identification of eosinophils and neutrophils in BAL fluid by flow cytometry. The number of total cells **(B)** , neutrophils **(C)** and eosinophils **(D)** in the BAL fluids. The number of eosinophils **(E)** and CD4⁺ T cells **(F)** in the lung tissues. **(G)** Intracellular cytokines expression in the lung tissues measured by flow cytometry after ex vivo stimulation. **(H)** Assessment of liver and kidney function. **(I)** H&E staining of liver sections (Scale bar = 50 μ m). Data are expressed as the mean \pm SD of individual groups of mice (n = 5 mice per group; * P < 0.05, ** P < 0.01, and *** P < 0.001, NS, not significant).

Figures

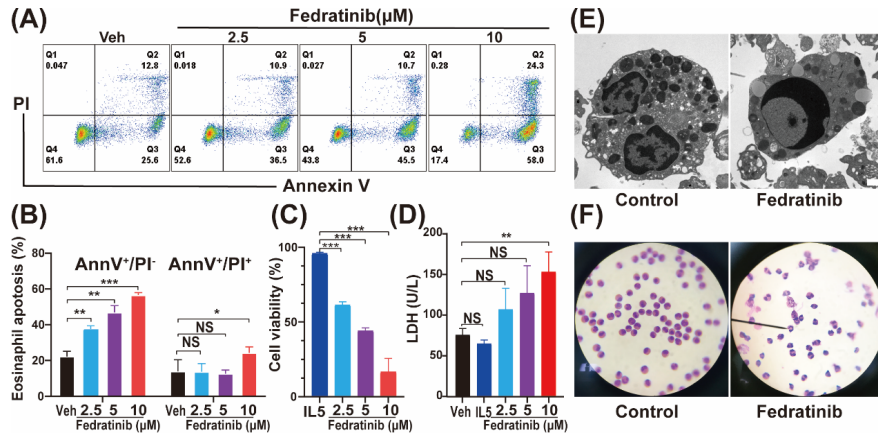


Figure 1. FDTN induces apoptosis of human eosinophils in a concentration-dependent manner. **(A, B)** Apoptosis in eosinophils was determined by flow cytometry ($n = 3$). **(C)** Eosinophil viability was assessed by CCK8 assay ($n = 3$). **(D)** LDH activity in culture supernatant was detected by automatic biochemical analyzer ($n = 3$). **(E)** Eosinophil morphology was analyzed by Transmission electron microscopy (TEM) (Scale bar = $1 \mu\text{m}$), FDTN-treated eosinophils show cellular shrinkage, nuclear condensation, chromatin condensation and along the nuclear membrane. **(F)** Representative morphology of eosinophils by Wright staining ($\times 1,000$ original magnification). Black needle pointed to two eosinophils with the apoptotic morphology. Data were expressed as mean \pm SEM of individual groups of peripheral blood eosinophils from 3 asthma patients. ($*P < 0.05$, $**P < 0.01$, and $***P < 0.001$).

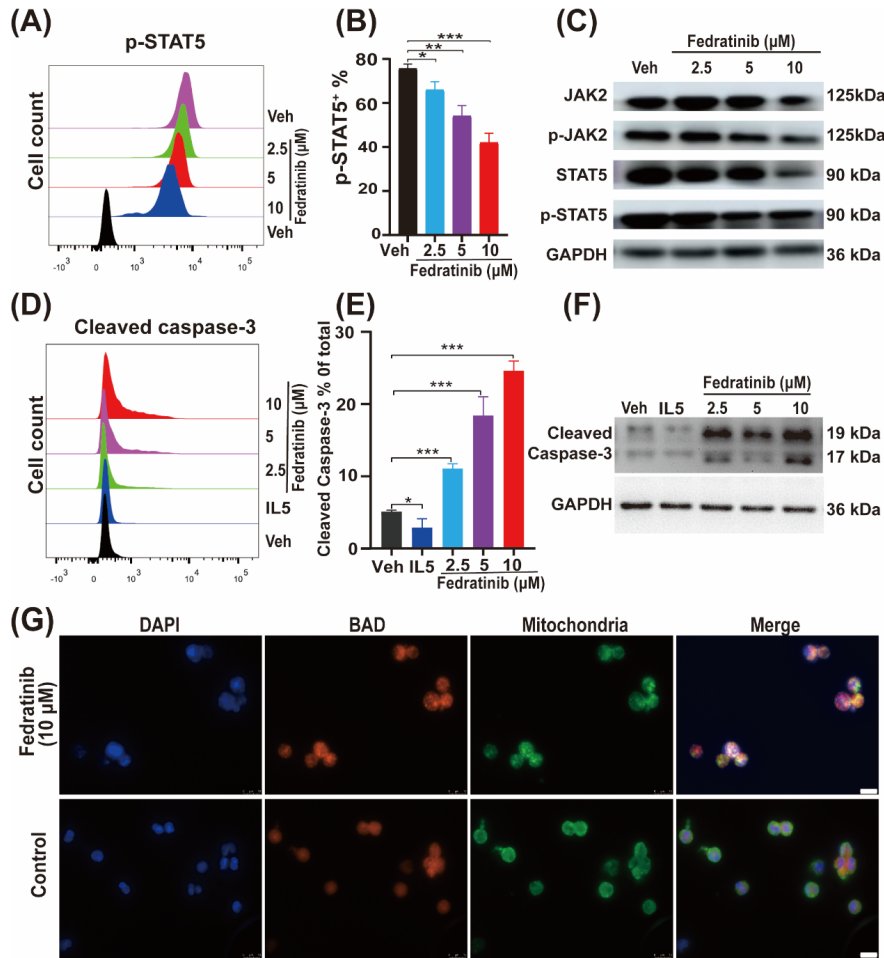


Figure 2. FDTN induces the intrinsic apoptosis pathway in human eosinophils. Peripheral blood eosinophils of asthma patients were isolated and incubated for 18h with either the vehicle or indicated amounts of FDTN. **(A)** Intracellular detection of p-SATA5 in eosinophils by flow cytometry. **(B)** The percentage of p-SATA5⁺ cells (n = 3). **(C)** Western blotting for JAK2 (125 kDa), STAT5 (90 kDa), p-STAT5 (90 kDa) and GAPDH (36 kDa). **(D)** Intracellular detection of cleaved caspase-3 in eosinophils by flow cytometry. **(E)** The cleaved caspase-3⁺ cell percentage (n = 3). **(F)** Western blotting for cleaved caspase-3 (17/19 kDa) and GAPDH (36 KD). **(G)** The colocalization (orange-yellow color) of BAD (Red color) and mitochondria (Green color) was assessed by fluorescence microscopy (Scale bar: 10 μm). Data were expressed as mean ± SD of each group. (**P* < 0.05, ***P* < 0.01, and *** *P* < 0.001).

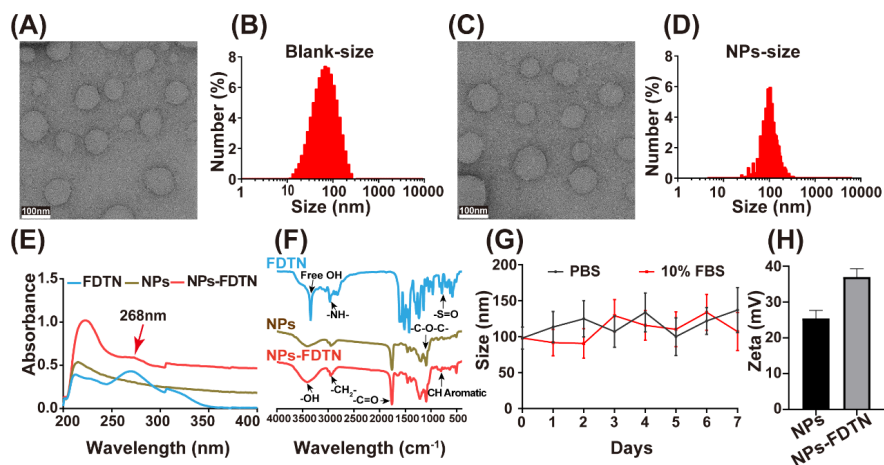


Figure 3. Characterization of nanoparticles. (A, B) TEM (Scale bar = 100 nm) image and size distribution of blank NPs. (C, D) TEM (Scale bar = 100 nm) image and size distribution of FDTN -loaded NPs.(E) The UV-vis spectra of free FDTN, NPs and NPs-FDTN in aqueous solution. (F) FTIR spectra of free FDTN, NPs and NPs-FDTN. (G) The stability of NPs in PBS/10% FBS.(H) The zeta potential of the NPs and NPs-FDTN.

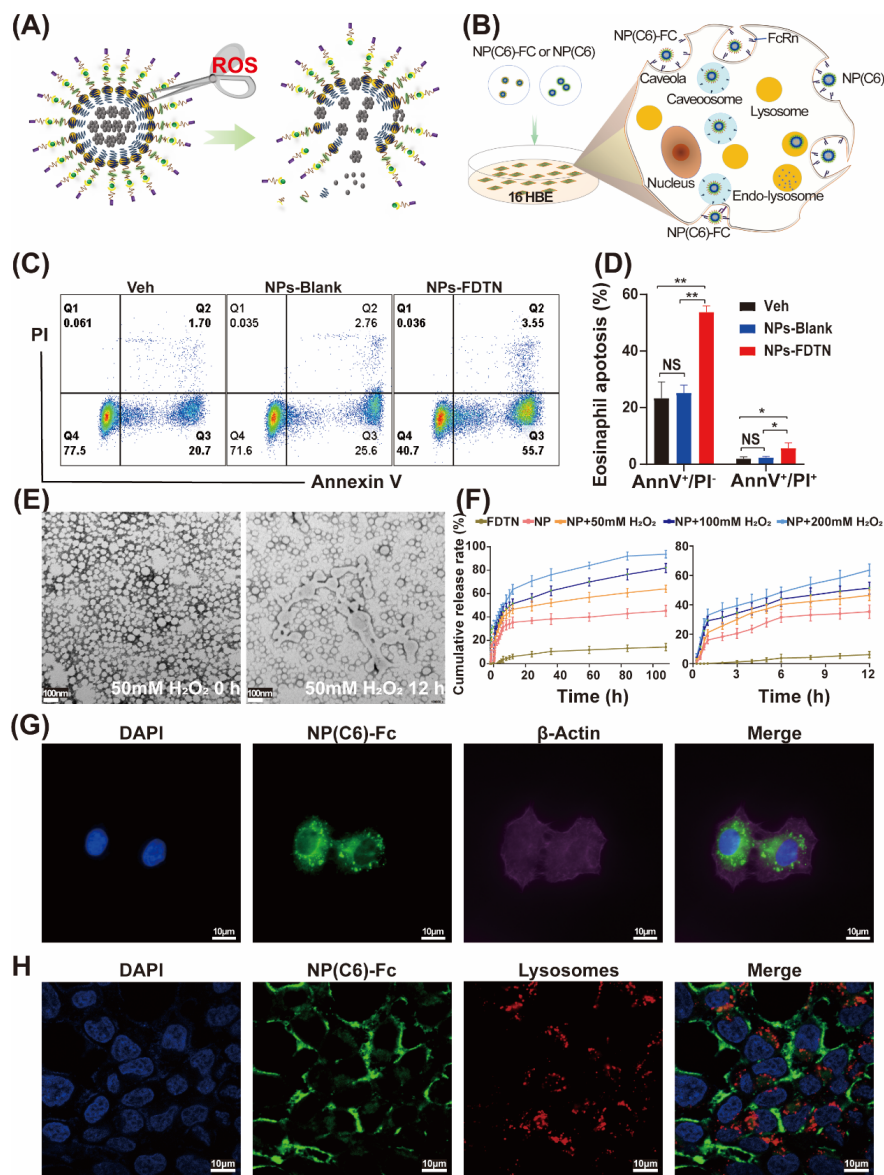


Figure 4. Biological availability of NP-Fc. **(A)** Schematic illustration of drug release from NPs triggered by ROS. **(B)** Schematic illustration of NP-Fc uptake by 16HBE cells. **(C, D)** Apoptosis in eosinophils treated by NP-Fc was determined by flow cytometry ($n = 3$). Data were expressed as mean \pm SD ($n = 3$). ($*P < 0.05$, $**P < 0.01$, and $***P < 0.001$). **(E)** TEM (Scale bar = 100 nm) image of NPs in 50 mM H_2O_2 at 0 h and 12 h. **(F)** FDTN release from NPs at different concentrations of H_2O_2 (0, 50, 100, and 200 mM) for 108 h, and the drug release curve within 12 h. **(G)** Intracellular tracking of NP(C6)-Fc in 16HBE. Images were taken after incubation with NP(C6)-Fc for 2 h and observed by fluorescence microscopy (Scale bar = 10 μm). NP(C6)-Fc (green), β -Actin (violet), nuclei (DAPI). **(H)** NP(C6)-Fc bypasses the lysosome assessed by confocal microscopy (Scale bar = 10 μm). NP(C6)-Fc (green), β -Actin (violet), LysoTracker[®] (red), nuclei (DAPI).

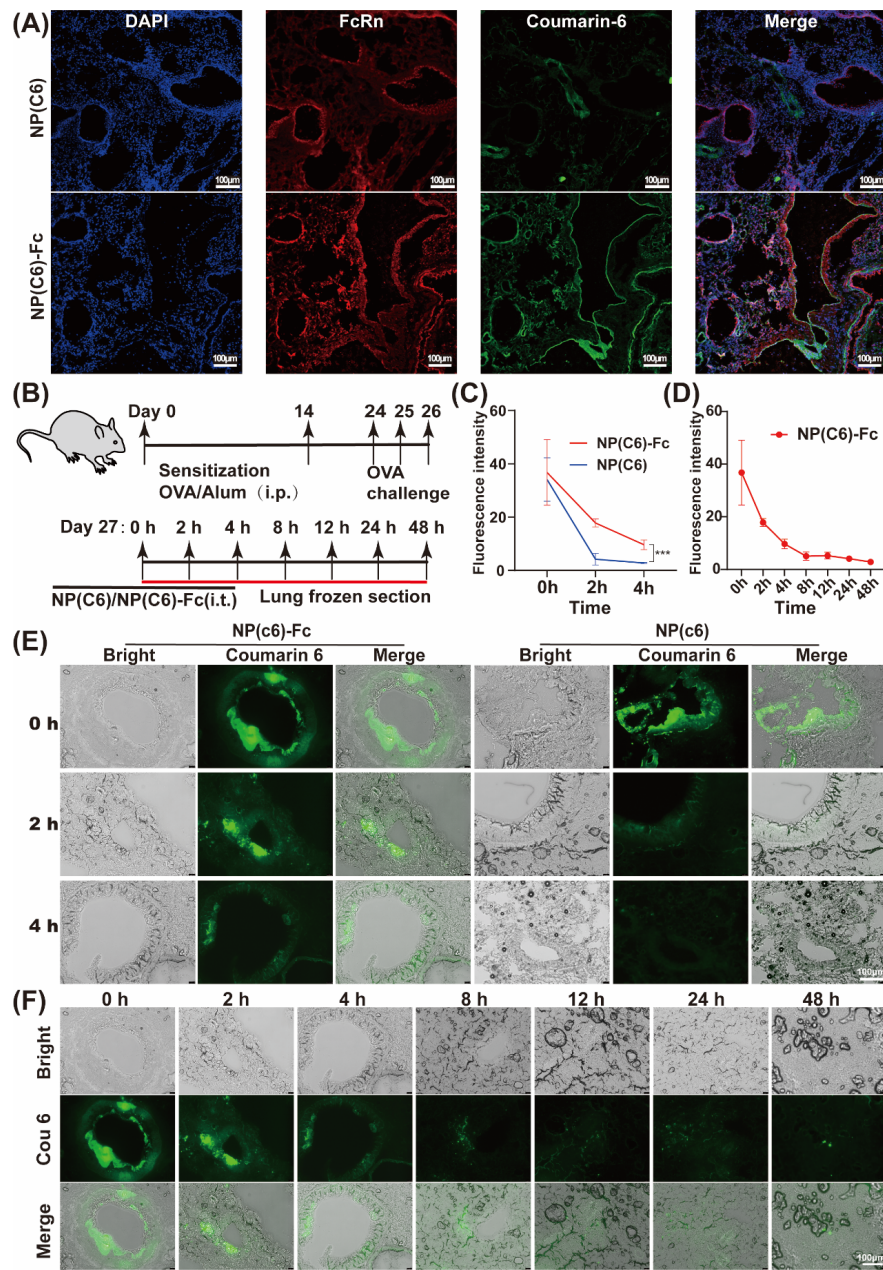


Figure 5. FcRn-targeting, transepithelial transport and residence time of NPs in the lung of mice. **(A)** FcRn-targeting of NP(C6) and NP(C6)-Fc in the frozen lung section by confocal microscopy (Scale bar = 100 μm). **(B)** Schematic illustration of NP(C6) and NP(C6)-Fc administration and lung sampling in the asthma model. **(C)** The comparative time-course fluorescence intensity between NP(C6) and NP(C6)-Fc. **(D)** The fluorescence intensity of NP(C6)-Fc in the lung sections at different time points. **(E)** Localization of NP(C6) and NP(C6)-Fc in the frozen lung section by fluorescence microscopy (Scale bar = 100 μm) at different time. **(F)** Localization of NP(C6)-Fc in the frozen lung section by fluorescence microscopy (Scale bar = 100 μm) at different time. Data were expressed as mean \pm SD ($n = 3$). (* $P < 0.05$, ** $P < 0.01$, and *** $P < 0.001$).

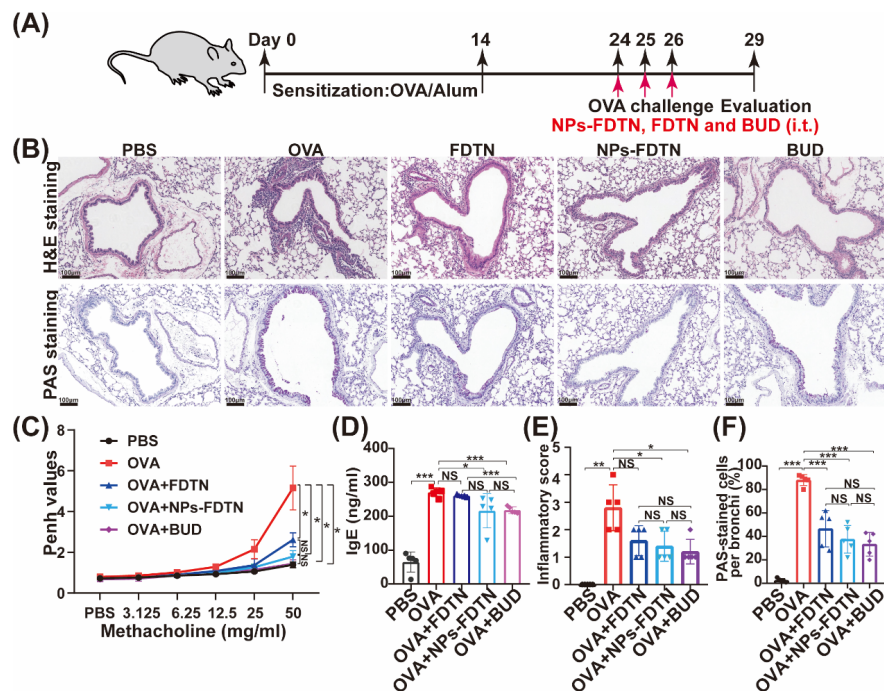


Figure 6. NPs-FDTN significantly attenuates the allergic airway inflammation. **(A)** Schematic illustration of the asthma model. **(B)** H&E- and PAS-stained lung sections (Scale bar = 100 μ m). **(C)** Airway hyper-responsiveness (AHR) measured with the Whole-body Plethysmograph System. **(D)** Serum IgE levels of different groups. **(E)** Inflammatory score of different groups. **(F)** PAS-stained cells per bronchi (%) of different groups. Data are expressed as the mean \pm SD of individual groups of mice (n = 5 mice per group; * P < 0.05, ** P < 0.01, and *** P < 0.001, NS, not significant).

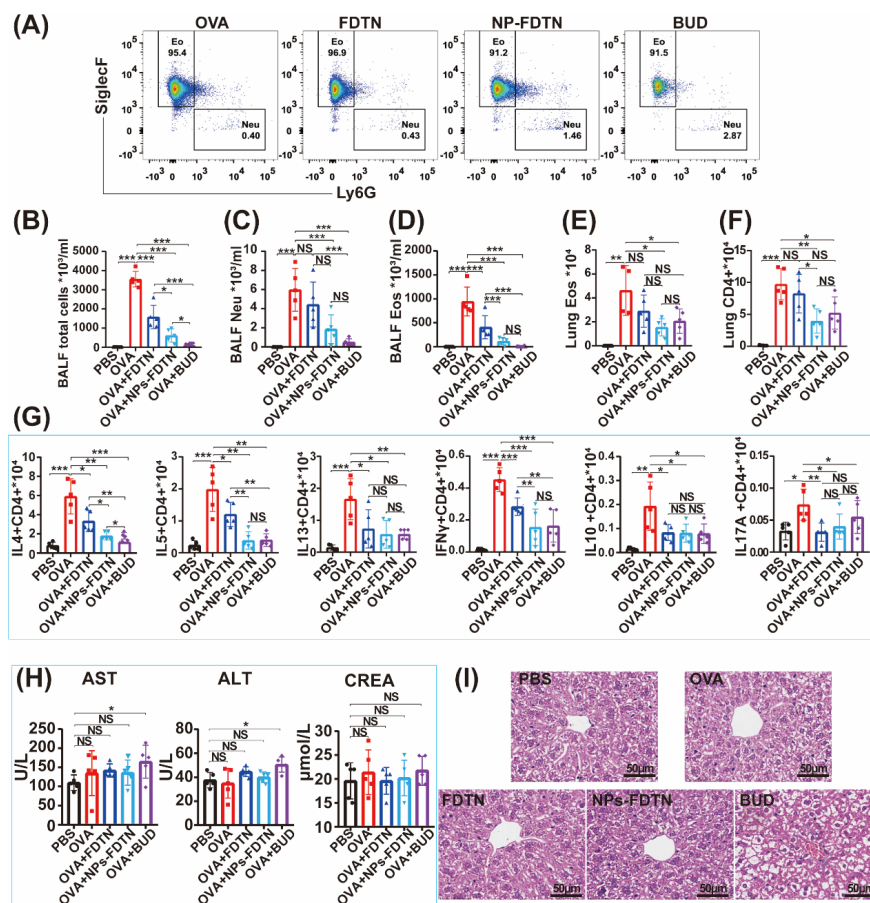


Figure 7. NPs-FDTN attenuate the immune response better than FDTN. **(A)** Identification of eosinophils and neutrophils in BAL fluid by flow cytometry. The number of total cells **(B)**, neutrophils **(C)** and eosinophils **(D)** in the BAL fluids. The number of eosinophils **(E)** and CD4 $^+$ T cells **(F)** in the lung tissues. **(G)** Intracellular cytokines expression in the lung tissues measured by flow cytometry after ex vivo stimulation. **(H)** Assessment of liver and kidney function. **(I)** H&E staining of liver sections (Scale bar = 50 μm). Data are expressed as the mean \pm SD of individual groups of mice (n = 5 mice per group; * $P < 0.05$, ** $P < 0.01$, and *** $P < 0.001$, NS, not significant).

Hosted file

Figure.zip available at <https://authorea.com/users/482634/articles/569114-fcrn-targeting-and-ros-responsive-fedratinib-incorporated-nanoparticles-alleviate-asthma-by-inducing-eosinophil-apoptosis>